

Sustained delivery of extracellular vesicles using UiO-66-NH₂ crosslinked hydrogel for accelerating chronic diabetic wound-healing

Wang Pan^{a,1}, Wenqing Wang^{a,1}, Peng Wang^b, Dong Chen^a, Shuo Liu^a, Likun Zhang^c, Ziyu Wang^d, Hui Yang^a, Yuanyuan Xie^a, Feifei Huang^a, Guohua Zhou^{c,*}, Bin Wang^{a,*}

^a Clinical Stem Cell Center, the Affiliated Drum Tower Hospital of Nanjing University Medical School, 321 Zhongshan Road, Nanjing 210008, China

^b State Key Laboratory of Pharmaceutical Biotechnology, Department of Sports Medicine and Adult Reconstructive Surgery, Nanjing Drum Tower Hospital, The Affiliated Hospital of Nanjing University Medical School, Nanjing 210008, China

^c Department of Clinical Pharmacy, Jinling Hospital, State Key Laboratory of Analytical Chemistry for Life Science & Jiangsu Key Laboratory of Molecular Medicine, Medical School of Nanjing University, Nanjing 210002, China

^d Department of Pathology, Nanjing Drum Tower Hospital, The Affiliated Hospital of Nanjing University Medical School, Nanjing 210008, China

ARTICLE INFO

Keywords:

Mesenchymal stromal cells
Extracellular vesicles
Metal-organic frameworks
Hydrogel
Sustained release
Chronic wound healing

ABSTRACT

Many patients with diabetes are suffering with chronic wounds due to their slow and disorganized healing process, which even lead to serious consequences such as amputation. Nowadays, extracellular vesicles derived from mesenchymal stromal cells (MSC-EVs) offer a potential strategy for chronic wound healing, whereas the rapid diffusion and degradation of MSC-EVs hampers the efficacy of wound repair. Herein, we proposed a novel MOF-based hydrogel by cross-linking hyaluronic acid (HA) with UiO-66-NH₂ (U6N). The HA-U6N hydrogel could be prepared rapidly with stable character, while the EVs affinity property of U6N was maintained well. This hydrogel allowed us enriching EVs conveniently and rapidly from cell supernatant. The U6N-based hyaluronic acid hydrogel with enriched EVs (HA-U6N-EVs) could markedly accelerate diabetic wound healing efficacy in rats attributing to the sustained release of EVs. Besides, we further showed the miRNAs in MSC-EVs involving in wound healing remained high abundance over 10 days, also demonstrating the superb sustained EVs delivery of HA-U6N hydrogels.

1. Introduction

The process of wound healing is intricate and dynamic, relying on the collaborative efforts of various cell types, such as keratinocytes, fibroblasts, and endothelial cells, which play crucial roles in epithelial regeneration, collagen remodeling, and angiogenesis [1]. However, chronic wounds, such as diabetic ulcers, often lead to more severe consequences due to their slow and disorganized healing process [2]. To address these challenges, researchers have extensively studied the potential of mesenchymal stromal cells (MSCs) in promoting wound healing [3,4]. Despite their therapeutic potential, MSCs-based therapy has some limitations, including a limited source and immunogenicity concerns [5,6]. Fortunately, there is a promising alternative in the form of extracellular vesicles derived from mesenchymal stromal cells (MSC-EVs). Extracellular vesicles are widely dispersed in body fluids, which could perform biological functions such as transmitting information,

removing intracellular components, and acting as biologically drug carriers that regulate physiological and pathological processes [7,8]. These vesicles are products and by-products of MSC culture, possessing similar biological effects to their parental cells [9]. Furthermore, MSC-EVs contain an abundance of miRNAs, which promote better wound healing performance by improving wound circulation, inducing angiogenesis, modulating inflammatory stress states, and cell communication [10–12]. Importantly, MSC-EVs are easier to obtain in large quantities and have lower immunogenicity compared to MSCs [13]. However, their rapid diffusion and short lifespan at injured sites necessitates the selection of an appropriate carrier to maintain their biological activity [14]. By harnessing the potential of MSC-EVs, researchers are exploring new avenues for effective wound healing treatments, offering hope for improved therapies in the management of chronic wounds like diabetic ulcers [7,15].

In addition to traditional materials, metal-organic frameworks

* Corresponding authors.

E-mail addresses: ghzhou@nju.edu.cn (G. Zhou), wangbin022800@126.com (B. Wang).

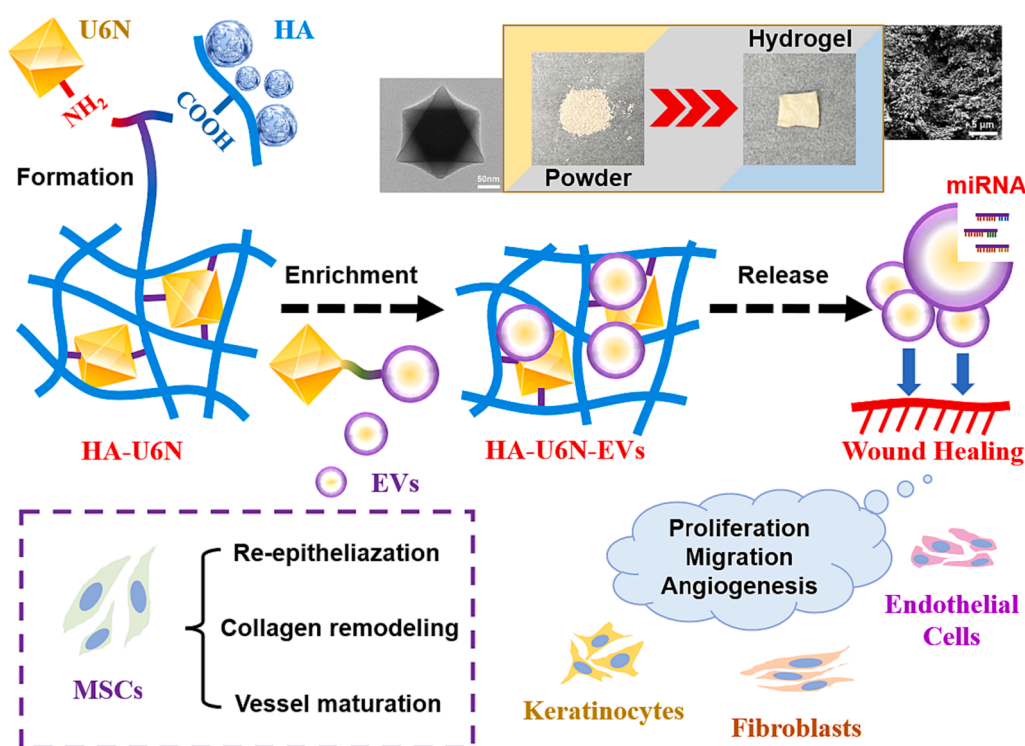
¹ Equal contribution to this study.

(MOFs) offer a unique class of organic–inorganic hybrid solids with infinite uniform frame structures, constructed by metal clusters and organic ligands [16,17]. The remarkable versatility of metal nodes and ligands, along with the diversity of connection combinations, bestows MOFs with an extensive range of structural variations, adjustability, and diverse physical and chemical properties [18,19]. Among the various MOFs reported, UiO-66-NH₂ (U6N) is commonly synthesized from ZrCl₄ and NH₂-H₂BDC. It has demonstrated superior water stability and an affinity for phosphate groups, making it particularly attractive for certain applications [20,21]. In our previous research, we have investigated the adsorption ability of U6N for extracellular vesicles (EVs). The zirconium clusters in U6N efficiently and specifically adsorb EVs by forming Zr–O–P coordination bonds with the phospholipids on the surface of EVs [22]. However, it is important to note that there are some challenges. To achieve EVs adsorption, the dried U6N crystals need to be fully dispersed in the buffer, which involves additional steps like centrifugation and resuspension, which may not be entirely favorable for preserving the integrity of both U6N and EVs. Fortunately, by combining primitive nanomaterials with appropriate dressings, we can leverage the advantages of both components. This opens up the exciting possibility of functionalizing MOFs into dressings for wound healing applications. With this approach, there is significant potential and promise for creating advanced wound dressings that can harness the unique properties of MOFs and enhance the wound healing process.

Currently, wound dressing remains a conventional yet widely used strategy for wound healing in clinical practice [11]. Biomedical hydrogels, in particular, hold great promise as biomaterials for delivering drugs and cells to aid in wound healing due to their structural similarity to the natural extracellular matrix [23,24]. To enhance the applicability of metal–organic frameworks (MOFs) and make them more effective, a feasible approach is to functionalize MOFs into gels with a porous structure, particularly by cross-linking them with biomedical hydrogels [25,26]. One excellent choice for hydrogel formation is hyaluronic acid (HA), a linear anionic polysaccharide composed of D-glucuronic acid and N-acetylglucosamine, known for its biocompatibility and positive impact on wound healing [27,28]. Furthermore, the superior embedding

ability of HA hydrogel makes it highly suitable for enriching and releasing MSC-EVs directly onto the wound surface, which is beneficial for wound healing [29]. However, the formation of HA hydrogels usually requires additional chemical modifications or cross-linking substances. Despite the potential advantages, there have been very few reports on HA-MOF hydrogels, not even involving UiO-66 hydrogel based on HA up to this point. Therefore, studying the formation and application of HA-U6N hydrogel represents an innovative and promising direction for future research.

In this study, we have utilized the unique properties of U6N crystals to develop a novel porous hydrogel that not only serves as a linker in the hydrogel but also acts as an adsorbent of EVs (Scheme 1). Specifically, the amino side on the surface of U6N allows it to bond with the carboxyl group in hyaluronic acid (HA), facilitating the convenient and rapid formation of HA-U6N hydrogel through the EDC/NHS reaction. Compared with the current HA hydrogel, our method avoided the chemical modification of HA, and realized the one-step formation of the gel at room temperature. Moreover, the EVs adsorption capability of U6N was utilized well because of the porous structure of HA-U6N and maintaining of zirconium clusters of U6N inside. By embedding U6N in the hydrogel, we extended the lifespan of EVs, enhancing their stability and continuous release over time, which is beneficial for wound healing. This resulted in the creation of a novel MSC-EVs dressing called HA-U6N-EVs. We investigated the EVs adsorption and release properties of HA-U6N to demonstrate the superior continuous releasing performance of the MSC-EVs dressing (HA-U6N-EVs). Furthermore, we evaluated the wound healing promotion capabilities of umbilical cord derived mesenchymal stromal cells (UCMSCs) and decidual derived mesenchymal stromal cells (DMSCs) by comparing their EVs to those from other cells in terms of cell proliferation, migration, and angiogenesis capacities *in vitro*. The results further emphasized the potential of MSC-EVs in wound healing. To validate the full potential of the HA-U6N-EVs composite hydrogel in an *in vivo* setting, we used diabetic rats with wounds on their backs for the healing experiment. Different treatment groups were set up, including rats treated with PBS, HA alone, HA containing DMSC-EVs, HA containing UCMSC-EVs, HA-U6N



Scheme 1. Illustration of MSC-EVs Sustained-Release Hydrogel Based on U6N (Denoted as HA-U6N-EVs) for accelerating chronic wound healing.

hydrogel, HA-U6N-DMSC-EVs composite hydrogel, and HA-U6N-UCMSC-EVs composite hydrogel. We harvested the skin tissues from these rats to verify the effects of HA-U6N hydrogel enriched MSC-EVs on wound healing promotion through histology and immunofluorescence assays. Additionally, we investigated the sustained release of miRNAs in MSC-EVs into the wounds, providing evidence of the continuous releasing performance of HA-U6N-EVs composite hydrogels *in vivo*. These findings offer promising insights into the potential therapeutic applications of the innovative HA-U6N-EVs composite hydrogel for wound healing.

2. Experimental section

2.1. Chemicals and materials

2-Aminoterephthalic acid ($\text{NH}_2\text{-H}_2\text{BDC}$) was purchased from Shanghai Maclin Biochemical Co., Ltd. (Shanghai, China). Ethanol, acetic acid, and Tween-20 were supplied by Nanjing Chemical Reagent Co., Ltd. (China). Zirconium chloride (ZrCl_4), sodium hydroxide (NaOH), sodium chloride (NaCl), Potassium chloride (KCl), N, N-dimethylformamide (DMF), disodium hydrogen phosphate (Na_2HPO_4), and potassium dihydrogen phosphate (KH_2PO_4) were supplied by Sino-pharm Chemical.

Reagent Co., Ltd. (China). 1-(3-Dimethylaminopropyl)-3-ethyl-carbodiimide hydrochloride (EDC) was purchased from Thermo Scientific (USA), and N-hydroxysuccinimide (NHS) was purchased from Sigma-Aldrich Co. (Germany). Hyaluronic acid was supplied by Xiya Reagent Co., Ltd. (China).

2.2. Synthesis of UiO-66- NH_2

UiO-66- NH_2 was synthesized based on a typical solvothermal protocol modified slightly by changing the amount of acetic acid [13]. ZrCl_4 (0.45 mmol) and 2-aminoterephthalic acid (0.45 mmol) were dissolved in 30 ml of DMF, and then 72 mmol of acetic acid was added into the solution. The solution was then transferred into a 50 ml teflon-lined autoclave, followed by heating at 120 °C for 24 h. After cooling to room temperature, the prepared product was washed three times with DMF and then dispersed in methanol for 3 days to remove the residual DMF molecules. Finally, the obtained product was washed with ethanol and then dried thoroughly under vacuum at 90 °C.

2.3. Formation of HA-U6N

HA-U6N was formed by hyaluronic acid and UiO-66- NH_2 . Briefly, 200 mg of HA was fully dissolved in 8 ml of deionized water, while 100 mg of U6N was distributed in 2 ml of water at the same time. Next, overdose of EDC and NHS was added into HA solution and U6N suspension respectively. Then these two parts were added into a 6 cm dish, followed with well stirring. After the hydrogel in the dish solidified through self-crosslinking, the product was freeze-dried for 48 h.

2.4. Measurement and apparatus

The crystallinity of the obtained products was determined by X-ray Diffraction (XRD, Thermo Fisher Scientific X'TRA). The morphology and binding construction analyses were performed by Transmission Electron Microscopy (TEM, Talos F200X). The Surface morphology and Energy Dispersive Spectrometer (EDS) analyses were performed by Scanning Electron Microscopy (SEM, Zeiss, Ultra Plus). Fourier Transform Infrared Spectroscopy (FT-IR) analyses were performed by a Nicolet iS10 FI-IR spectrometer. The X-ray Photoelectron Spectroscopy (XPS) spectra before and after loading EVs were analyzed by Thermo escalab 250XI, and the calibration of all the binding energies was performed by the C 1 s peak (284.8 eV). The quantification of EVs were performed by Nanoparticle Tracking Analysis (NTA) using ZetaView (Particle Metrix,

Germany).

2.5. Cell culture and supernatant acquisition

Human foreskin fibroblasts (HFF) were obtained from the departments of andrology, Nanjing Drum Tower Hospital. Human umbilical vein endothelial cell (HUVEC), human immortalized epidermal cells (HaCat), decidua mesenchymal stromal cells (DMSC) and umbilical cord mesenchymal stromal cells (UCMSC) were provided by clinical stem cell center from Nanjing Drum Tower Hospital. All umbilical cord and decidua samples were taken after informed and written consent, and the study was approved by the Research Ethics Board of Nanjing Drum Tower Hospital (permit number 2017-161-01). HaCat cells were cultured in high-glucose DMEM medium contain with 10 % FBS and 1 % penicillin-streptomycin (Corning Incorporated, USA), and incubated in a cell culture chamber (Thermo Fisher Scientific) containing 5 % CO_2 at 37 °C. HFF, HUVEC, DMSC, and UCMSC were cultured in low-glucose DMEM medium contain with 10 % FBS, 1 % penicillin-streptomycin, and 0.05 % bFGF (T&L Biotechnology Co.,Ltd.), which were also incubated in a cell culture chamber containing 5 % CO_2 at 37 °C.

Supernatants of each cell type were acquired using the same procedure. Firstly, cells were cultured to approximately 80 % confluency. The medium was then discarded and cells were washed by normal saline gently. Next, each culture vial was added with 8 ml normal saline, and incubated for 24 h. Finally, supernatant from vials was collected after $4000 \times g$ centrifugation for 10 mins. Additionally, qEVoriginal / 35 nm (SP5, IZON, New Zealand) was utilized to obtain purified EV in need.

2.6. EVs bioactivities investigation in vitro

1) Cell Proliferation Test

CCK-8 kit (Vazyme Biotech Co., Ltd, China) was utilized to evaluate the cell proliferation promotion. The HFFs were seeded in a 96-well plate at 6000 cells per well and kept in 200 μL of DMEM medium that contained 10 % FBS, while the number of HUVECs and HaCats were 4000 per well, respectively. The cells were then treated with 50 μL of various types of supernatants or elution products per well (HFF, HUVEC, HaCat, DMSC, and UCMSC) for 48 h. Each group had triple parallels. Cells treated with 50 μL of PBS (10 mM) as the control group. Afterwards, the medium was discarded and 100 μL of 10 % CCK-8 solution with a culture medium was added to each well. Then, the plates were incubated for 2 h at 37 °C. Finally, the optical density at 450 nm was read using a microplate reader (Multiskan FC, Thermo Scientific), and the results were then statistically analyzed and plotted.

Cells treated with PBS were utilized as negative control; cells treated with HFF-EVs, HUVEC-EVs, HaCat-EVs, DMSC-EVs, and UCMSC-EVs were used as experimental groups. The cell proliferation percentage were represented by the ratio of OD value between each group and negative control.

2) Transwell Migration Analysis

The cells (2×10^4 cells per well) were suspended in 100 μL of DMEM medium that contained 10 % FBS and then seeded on the upside of the transwell insert (Corning Incorporated, USA). Next, each well was filled with 1 ml of DMEM medium that contained 10 % FBS, and 200 μL of various types of supernatants or elution products per well (HFF, HUVEC, HaCat, DMSC, and UCMSC). Each group had triple parallels. Medium mixed with 200 μL of PBS (10 mM) as the control group. After 48 h incubation (5 % CO_2 , 37 °C), the cells that did not migrate were removed by using a cotton swab, and the cells that migrated to the downside of Transwell insert were stained with crystal violet staining solution (Beyotime, China) and imaged under a microscope (Carl Zeiss, Oberkochen, Germany).

Normal cell culture medium contained 20 % PBS was added into the

well as control, while the medium contained 20 % cell supernatant of HFF, HUVEC, HaCaT, DMSC, UCMSC, and 20 % elution products from corresponding HA-U6N-EVs composite hydrogels as experimental groups.

3) Microvessels Formation Analysis

50 μL of growth factor-reduced Matrigel (BD Biosciences, USA) was added into each well of the 96-well plate and then place in a 37 °C incubator for 1 h until solidification. Next, HUVECs (1.5×10^4 cells per well) were seeded on the solidified Matrigel substrates and cultured in 200 μL of DMEM medium and then added with 50 μL of various types of supernatants or elution products per well (HFF, HUVEC, HaCaT, DMSC, and UCMSC) or with PBS as control. After 24 h of incubation (5 % CO_2 , 37 °C), the cells were imaged using microscopy (Carl Zeiss, Oberkochen, Germany).

Normal cell culture medium contained 20 % PBS for 24 h as negative control, while the medium contained 1 % HA was represented as placebo control group; medium contained 20 % cell supernatant of HFF, HUVEC, HaCaT, DMSC, UCMSC, and 20 % elution products from corresponding HA-U6N-EVs composite hydrogels as experimental groups.

2.7. EVs releasing investigation

Firstly, EVs obtained from supernatant were diluted to 10^9 particles/mL. Meanwhile, HA-U6N was divided into appropriate size for testing. Next, 1 ml of quantitative EVs and on piece of HA-U6N were added into each tube. After 48 h, the supernatants were discarded, and 1 ml of PBS with different concentration (0, 2.5, 5, 7.5, and 10 mM) was added in order to elute EVs from the HA-U6N-EVs composite hydrogel. Afterwards, the elution products were collected after 24 h, while the new PBS buffer was added for further eluting. After continuous collection, elution products (24, 48, 72, 96, and 120 h) would be obtained from each group, respectively. EVs in every tube would be qualitative by Western blotting, and quantitative using ZetaView.

For western blotting analyses, 0.8 ml of each sample was freeze-dried and then resuspended in 80 μL of PBS (10 mM), followed by boiling 5 mins after adding 20 μL of $5 \times$ SDS loading buffer.

Afterwards, 20 μL of each sample was separated by SDS-PAGE, followed by transferring to polyvinylidene difluoride (PVDF) membranes (Merck Millipore, USA). Next, each PVDF membrane was blocked with 5 % BSA for 2 h, and then primary antibody (TSG-101, A5789, 1:2000, Abclonal Technology Co., Ltd, China) was utilized to incubate with PVDF membranes at 4 °C overnight. Finally, the washed membranes were incubated for 1 h with HRP-labeled Goat Anti-Rabbit IgG (A0208, 1:1000, Beyotime Biotech Inc, Shanghai, China) to allow the protein being detected by ECL chemiluminescence (E412-01, Vazyme Biotech Co., Ltd, China).

For nanoparticle tracking analysis (NTA), each sample was diluted to appropriate concentration, and followed by smoothly injecting into the Zetaview. Each sample was detected for three times.

2.8. Wound healing evaluation in vivo

Female rats of 4–6 weeks were chosen in this study. Streptozotocin (STZ, Sigma-Aldrich, USA) was used to induce diabetic model. In detail, STZ was freshly dissolved in citric acid sodium citrate buffer (100 mM) to configure a final concentration of 12 mg/mL solution. The rats which had been fasted for 12 h were intraperitoneal injected STZ (60 mg/kg) afterwards. The blood glucose of rats was monitored after 1 week, and the rats with blood glucose higher than 16.67 mM were chosen for subsequent experiments. Rats in blank group were inject with citric acid sodium citrate buffer instead of STZ. After shaving the anaesthetized rats, two full-thickness excisional skin wounds (10×10 mm in width and length) were constructed on both sides of the spine, respectively. The rats were randomly divided into groups and only treated one time as

following: 1) NC group (diabetic rats treated with 200 μL of PBS each wound); 2) HA group (diabetic rats treated with 200 μL of 2 % HA each wound); 3) HA-DMSC-EVs group (diabetic rats treated with 200 μL of 2 % HA contained 10^{10} DMSC-EVs each wound); 4) HA-UCMSC-EVs group (diabetic rats treated with 200 μL of 2 % HA contained 10^{10} UCMSC-EVs each wound); 5) HA-U6N group (diabetic rats treated with one piece of HA-U6N hydrogel each wound); 6) HA-U6N-DMSC-EVs group (diabetic rats treated with one piece of HA-U6N-DMSC-EVs composite hydrogel contained 10^{10} DMSC-EVs each wound); 7) HA-U6N-UCMSC-EVs group (diabetic rats treated with one piece of HA-U6N-UCMSC-EVs composite hydrogel contained 10^{10} UCMSC-EVs each wound). After the wound treatment, additional sponges soaking with PBS (10 mM) were putted around the wounds to provide elution environment at group 6 and 7, while one piece of 3 M thin dressing was covered onto the each wound to prevent the detaching of hydrogel and sponges. At days 0, 5, and 10 post-operations, the wounds were photographed and measured with vernier calipers. Finally, the rats were sacrificed at day 5 and day 10, and wounds were cut out with carefully preservation. The wound healing rate was calculated using following formulation [30]:

$$\text{Wound healing rate (\%)} = (\text{length}_i \times \text{width}_i / \text{length}_0 \times \text{width}_0) \times 100 \%; i = 5, 10$$

The animal experiments were approved by the Research Ethics Board of Nanjing Drum Tower Hospital, the Affiliated Hospital of Nanjing University Medical School (approval no.2021AE02019).

2.9. Histology staining

After wound fixation by paraformaldehyde, the skin tissues were embedded in paraffin for hematoxylin and eosin (H&E) and masson staining.

1) H&E staining

The paraffin sections of skin tissue were firstly dewaxed by xylene for 3 times, and rehydrated by ethanol solutions with different concentrations in sequence. Next, samples were stained by hematoxylin about 5 mins, followed by washing with hematoxylin differentiation solution for 5 s. Then the samples were soaked in weak alkali solution for several mins until the nucleus in tissues turning blue. Afterwards, the samples were stained by eosin for 1 min. The stained sections were dehydrated and transparent again, followed by sealing at last.

2) Masson staining

The paraffin sections of skin tissue were dewaxed and rehydrated as pretreatment correspondingly. Afterwards, tissues were handled according to the protocol of masson staining kit (BA4079A, Baso, China). In detail, samples were stained by weigert iron hematoxylin for 8 mins, followed by washing with differentiation solution for several seconds. Next, the samples were stained by ponceau acid fuchsin dye for 8 mins. Afterwards, samples were incubated with phosphomolybdic acid for 5mins, and aniline blue dye for 4 mins successively. The stained tissues were then washed by 1 % acetic acid for several times. At last, the samples were dehydrated, transparent, and sealed in sequence.

2.10. Immunofluorescence

After dewaxing and rehydration of samples, the sections of paraffin tissues were implemented for antigen retrieval in high temperature. Next, samples were permeated with 0.5 % triton and then blocked with PBS contained 5 % serum for 1 h at room temperature. Afterwards, samples were incubated overnight with 0.2 % of corresponding antibody at 4 °C. The samples were washed gently after removing the antibody,

and then incubated for 2 h at room temperature with the working solution which had mixed two fluorescent secondary antibodies together. Finally, DAPI tablets (ab104139, Abcam) were dropped on the surfaces of the samples, and the slices were sealed.

The primary antibodies were used as follows: Keratin-14 (ab7800, Abcam), Keratin-5 (ab52635, Abcam), α -SMA (ab7817, Abcam), and CD-31 (ab222783, Abcam).

The secondary antibodies were used as follows: Alexa Fluor 488 Goat anti-Mouse IgG (A-11001, Invitrogen), Alexa Fluor 568 Goat anti-Rabbit IgG (A-11011, Invitrogen).

2.11. miRNA abundance analyses

The abundance of miRNAs was evaluated in EVs samples and animal skin samples respectively. Firstly, samples were lysed, and the total RNAs were extracted using RNA-easy Isolation Reagent (R701, Vazyme Biotech Co.,Ltd, China). Afterwards, the miRNA 1st Strand cDNA Synthesis Kit (MR-201, Vazyme Biotech Co.,Ltd, China) was used to synthesize cDNA library, accordingly to the manufacturer's instructions. In detail, each tube contained 2 μ g of RNA, 10 μ L of 2 \times miRNA RT Mix, 2 μ L of HiScript miRNA Enzyme Mix, then up to 20 μ L with RNase-free ddH₂O. The tubes were incubated for 1 h at 37 $^{\circ}$ C, followed by enzyme inactivation at 85 $^{\circ}$ C for 5 min.

For qPCR quantification, each tube contained 2 μ L of cDNA, 10 μ L of ChamQ Universal SYBR qPCR Master Mix (Q711-02, Vazyme Biotech Co.,Ltd, China), 0.5 μ L of corresponding forward and reverse primer respectively, and up to 20 μ L with 7 μ L ddH₂O.

The abundance of miRNAs in skin samples was compared between control and each experimental group as follow:

$$\text{Relative Fold Change} = 2^{-(\Delta C_{tX} - \Delta C_{tN})}$$

ΔC_t represented the value of $C_{tU6snRNA}$ minus C_{tmiRNA} in each group, whereas the ΔC_{tN} represented the result in negative control group, and ΔC_{tX} represented the result in each experimental group.

The specific primer for each microRNA, U6 snRNA, and GAPDH was designed according to Table 1.

2.12. Statistical analysis

At least three replicates of each data were listed as the mean \pm standard derivation (SD) of for each experiment. Then data were presented and analyzed by unpaired parametric test with Welch's correction through the software GraphPad Prism (8.0.2, GraphPad Software, USA), and $p < 0.05$ was considered statistically significant.

3. Result and discussion

3.1. Characterization of EVs adsorption properties by U6N

In order to investigate the adsorption ability of U6N crystals towards EVs, we collected cell supernatant following the procedure described in

Fig. 1A, whereas the EVs characterizations indicated the similar morphology and concentration after starvation with culture medium or saline (Fig. S1). Utilizing quantitative detection by Nanoparticle Tracking Analysis (NTA), we observed the EVs concentration in the supernatant was significant decreased after U6N incubation, indicating a superior adsorption ability of U6N towards EVs (Fig. 1B). Transmission Electron Microscopy (TEM) results exhibited highly monodisperse octahedral U6N crystals with a smooth surface, measuring approximately 200 nm in size (Fig. C1). Upon blending U6N with EVs, we captured images of the binding configuration between U6N and EVs (Fig. C2). To further explore the binding mechanism, X-ray Photoelectron Spectroscopy (XPS) was employed, revealing that the binding energy of the Zr element decreased slightly because of the increasing density of the external electron cloud of Zr atoms given by the lone-pair electrons of P–O, coinciding with the appearance of a phosphorus characteristic peak after the extraction of EVs (Fig. 1D and E). These findings collectively demonstrated that U6N possesses the capability to effectively and specifically adsorb EVs, attributed to the affinity of zirconium clusters towards phosphate groups on the surface of EVs. Furthermore, the competitive binding of zirconium clusters between phosphates group and phospholipid proposes the elution of EVs from U6N by introducing PBS [20,21].

3.2. Preparation and characterization of HA-U6N

Recent interventions for chronic wound healing, such as diabetic ulcer, have pay more attention on the development of therapies based on extracellular components, biomaterials, and stromal cells as well as tissue engineering products [31]. Therefore, we developed a porous hydrogel by cross-linking U6N and HA, aiming to achieve efficient enrichment and continuous release of EVs. The process involved activating the carboxyl group in HA using EDC, allowing the amidation reaction to take place with the amino group on the surface of U6N. Despite of the viscous fluid-like hydrogels, HA-U6N hydrogel was formatted in solid hydrogel construction with stable structure because of the cross-linking between carboxyl groups in hyaluronic acid and amino groups on the surface of U6N crystals. Scanning Electron Microscopy (SEM) results revealed that the surface of HA-U6N hydrogel exhibited a slightly rough texture with numerous mesopores. Additionally, the inner part of the hydrogel showed a fibrous structure, indicating effective cross-linking between U6N and the hydrogel matrix (Fig. 2A). Correspondingly, the high-resolution TEM images also investigated the cross-linking state of U6N crystals inside of the hydrogel (Fig. S2). Furthermore, Energy Dispersive X-ray Spectroscopy (EDS) analysis confirmed that U6N crystals were embedded within the HA-U6N hydrogel, especially in the inner part of the hydrogel (Table S1). The structural integrity of HA-U6N was well-preserved even after further swelling and freeze-drying (Fig. 2B). The HA and U6N mixture without cross-linking would be dissolved in 1 day, whereas the HA-U6N hydrogel could retain stable for a long time (Fig. S3). FT-IR analysis demonstrated the extreme high characteristic peaks among 1647.9 cm^{-1} and 1564.5 cm^{-1} , which

Table 1
Sequences of the primers utilized for qPCR.

#	Name	Forward Primer	Reverse primer
1	hsa-miR-21-5p	TAGCTTATCAGACTGATGTGA	Universal reverse Q primer in miRNA 1st Strand cDNA Synthesis Kit
2	hsa-miR-22-3p	TTGACGGTCAACTTCTTGACA	
3	hsa-miR-23a-3p	TAGTGTAAACGGTCCCTAAAGG	
4	hsa-miR-27a-3p	AAGTGTCAACGATTCAAGGCG	
5	hsa-miR-125b-5p	TCCCTGAGACCCTAACTTGTGA	
6	hsa-miR-135b-5p	TATGGCTTTTCATTCTATGTGA	
7	hsa-miR-146a-5p	ACTCTTGACTTAAGGTACCCAA	
8	hsa-miR-150-5p	TCTCCCAACCCCTGTACCACTG	
9	has-miR-499a-3p	AACATCACAGCAAGTCTGTGCT	
10	U6 snRNA	ACACGCAAAATTCGTGAAG	GTTGAAGTCGCAGGAGACAA
11	GAPDH	ACAACTTTGGCATTGTGGAAG	

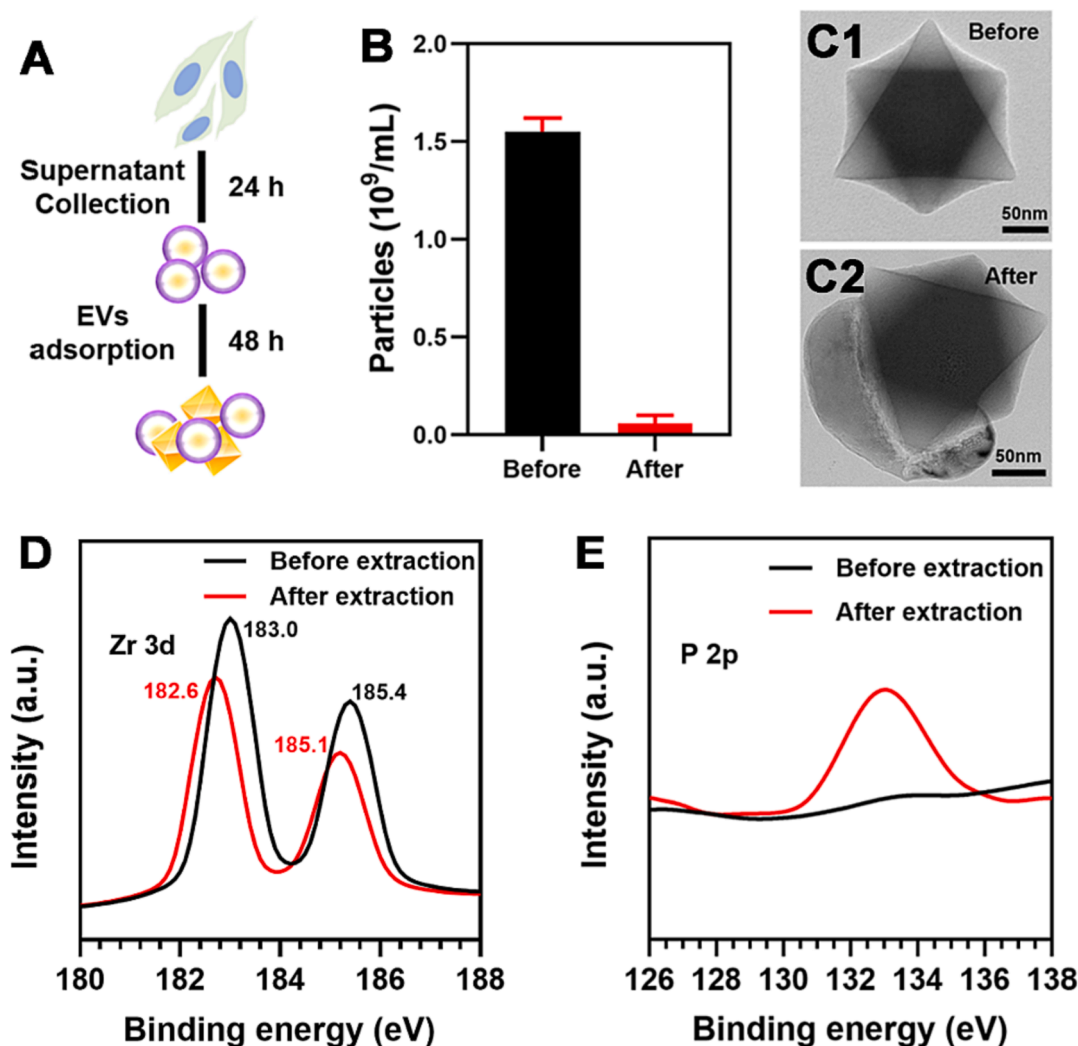


Fig. 1. Adsorption and characterization of U6N-EVs. (A) Schematic representation of EVs adsorption by U6N from cell supernatants. (B) EVs concentration in cell supernatants before and after U6N adsorption. (C) Representative TEM images of U6N construction (C1) before and (C2) after EVs adsorption. (D, E) XPS analysis of U6N before and after EVs adsorption: (D) Zr 3d and (E) P 2p.

were corresponding to the $\nu_{\text{C=O}}$ and δ_{NH} from primary amide. Moreover, the characteristic peak of $\nu_{\text{C=O}}$ was shifted from 1624.7 cm^{-1} to 1647.9 cm^{-1} , while the characteristic peak of δ_{NH} was shifted from 1573.4 cm^{-1} to 1564.5 cm^{-1} after synthesis, respectively. The peak at 2723.7 cm^{-1} could be attributed to the enhancement of ν_{OH} from carboxylic acids through hydrogen bond after hydrogel formation. This result indicated the formation of an amide bond between the amino group on U6N and the carboxyl group in HA (Fig. 2C). Additionally, the characteristic peaks of U6N were maintained in HA-U6N, indicating that the crystallinity and integrity of U6N were preserved within the hydrogel (Fig. 2D). Moreover, thermogravimetric analysis of HA-U6N indicated the possessing thermodynamic characteristics of both HA and U6N. The weight loss within $350\text{ }^{\circ}\text{C}$ could be attributed to the decomposition of HA organic structure, and the weight loss curve within $650\text{ }^{\circ}\text{C}$ was slightly delayed compared but similar with that of U6N (Fig. S4). Based on these comprehensive characterizations of HA-U6N, it can be inferred that the hydrogel inherited appropriate properties from U6N without structure destruction. These suggesting its potential for EVs adsorption and continuous release, which is crucial for the development of an effective dressing for wound healing. As shown in Fig. S5, the abundant phosphorus indicated the EVs extraction ability of HA-U6N hydrogel, relatively.

Therefore, the EVs releasing condition was investigated

subsequently. Previous studies have demonstrated the nucleic acid which is bond on the surface of U6N could be eluted by phosphate through competitive combination [20]. Similarly, EVs binding in HA-U6N would be eluted with the infiltration of phosphate inside the hydrogel. This process is relatively slow, resulting in a continuous release of EVs adsorbed in HA-U6N. As shown in Fig. 2E, the release of EVs was depend on the concentration of PBS in the elution buffer. In detail, few number of EVs were released into the supernatant without PBS even after 120 h of soaking. By contrast, more EVs were detected in the supernatant along with the increasing concentration of PBS. In summary, it is completely feasible to utilize HA-U6N for EVs adsorption and continuous releasing.

Notably, this innovative approach of using HA-U6N as a composite hydrogel to efficiently enrich and release EVs holds great promise for advanced wound healing therapies. The stable and porous nature of the hydrogel, combined with the specific adsorption of EVs, allows for the sustained and targeted delivery of therapeutic factors, making it an attractive candidate for addressing the challenging issue of chronic wound healing.

3.3. Cell viability promotion of EVs in vitro

Having established the superior EVs adsorption and continuous

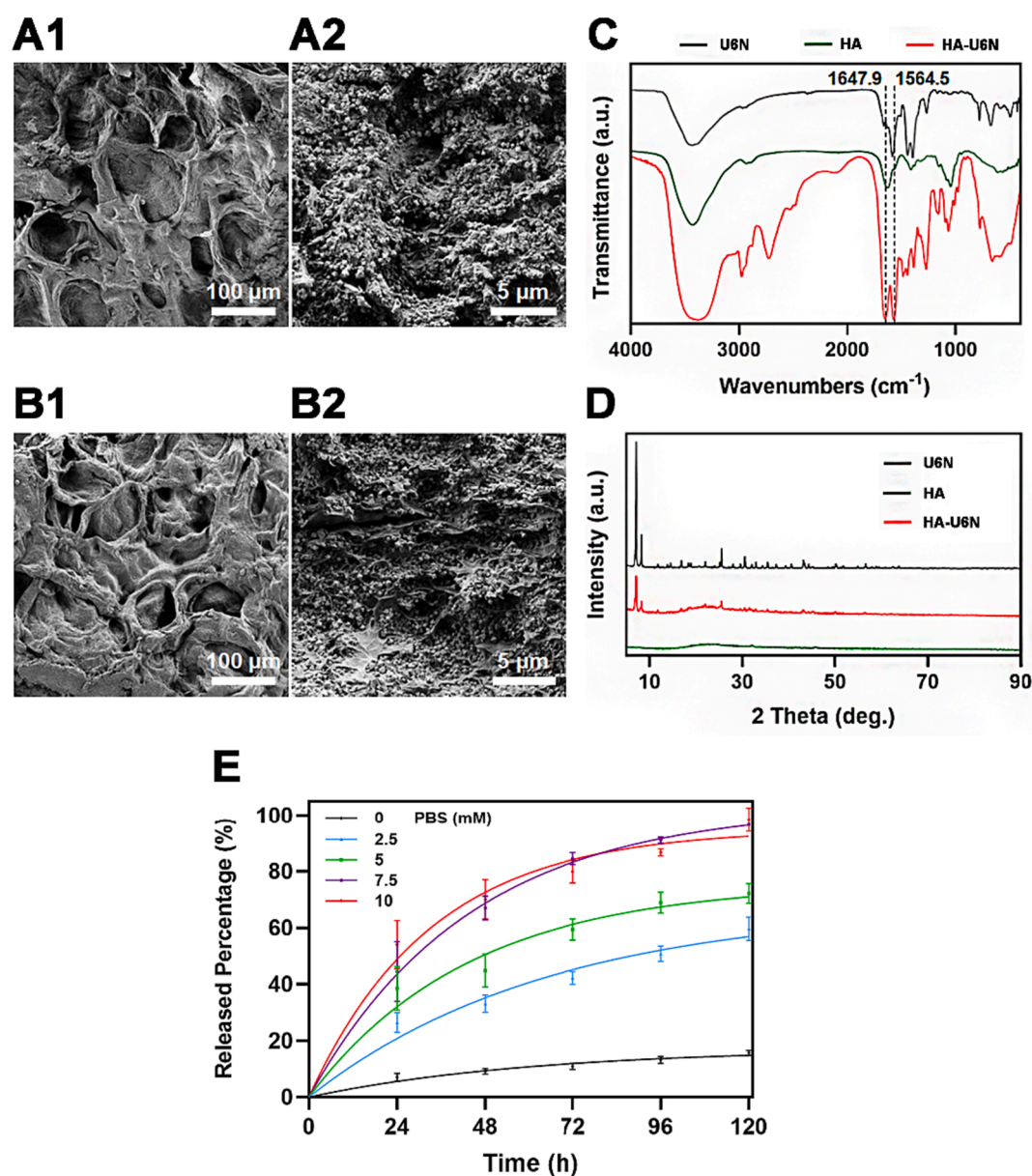


Fig. 2. Characterization of HA-U6N hydrogel and investigation of HA-U6N-EVs composite hydrogel for the continuous release of EVs. (A and B) SEM images of HA-U6N (A1 and A2) freeze-dried after preparation and (B1 and B2) freeze-dried after swelling. (C) FT-IR spectra, and (D) XRD patterns of HA, U6N, and HA-U6N hydrogel. (E) Continuous releasing quantification of EVs from HA-U6N-EVs composite hydrogel by different concentration of PBS. Results were mean \pm SD ($n = 3$).

releasing ability of HA-U6N, we proceeded to investigate the feasibility of the HA-U6N-EVs composite hydrogel *in vitro*. To do this, the effects of cell viability were compared by adding the elution products from HA-U6N-EVs with those from the original supernatant. Additionally, we aimed to determine whether EVs derived from mesenchymal stromal cells (MSCs) could play more significant roles in wound healing compared to other cell types involved in the process, such as fibroblasts, endothelial cells, and keratinocytes. We first evaluated the influences of different types of supernatants on cell proliferation. After a 48-hour incubation period, significant differences were observed in most groups compared to the control group. Specifically, UCMSC-EVs exhibited the highest promotion of fibroblast (HFF) proliferation, surpassing the effects of other groups. The promotion effects of EVs were consistent with the results of unenriched groups even after the enrichment of HA-U6N. On the other hand, DMSC-EVs and UCMSC-EVs showed the best promotion of endothelial cell (HUVEC) proliferation before and after enrichment by HA-U6N, respectively. As for keratinocytes (HaCat), DMSC-EVs proved to be the most effective in promoting

proliferation, regardless of enrichment or not (Fig. 3A). Cell migration is another critical aspect of wound healing. Transwell results indicated that EVs derived from DMSCs and UCMSCs promoted cell migration better than other groups across all three cell types, with HaCat cells exhibiting the most substantial improvement. The migration promotion of EVs was further validated through quantification of each group (Fig. 3B). Furthermore, we assessed vessel formation using the tube formation assay. The results revealed that UCMSC-EVs demonstrated the highest promoting ability for vessel formation in endothelial cells (Fig. 3C). These findings collectively indicated the potent wound healing properties of UCMSC-EVs and DMSC-EVs. MSC-EVs demonstrated significant promotion of cell viabilities among fibroblasts, endothelial cells, and keratinocytes when applied at the dose level in the cell supernatant. Moreover, EVs eluted from the HA-U6N-EVs composite hydrogel achieved similar results compared to those from the cell supernatant. These findings strongly revealed that the bioactivities of EVs from HA-U6N-EVs were well retained and released at a controlled and gentle dose. The enriching and releasing properties of porous hydrogel allowed for

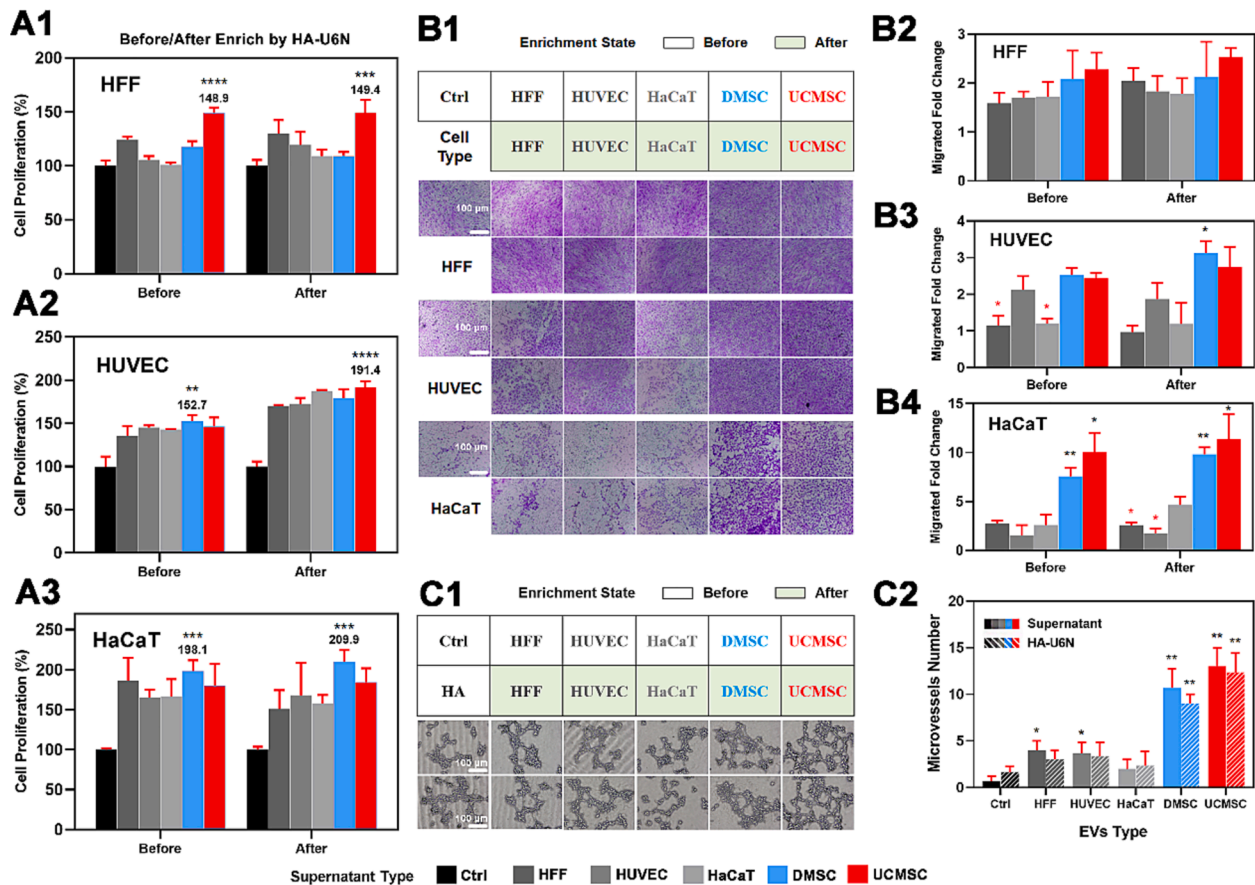


Fig. 3. *In vitro* bioactivities of EVs. (A) Proliferation of (A1) fibroblast, (A2) endothelial, and (C) keratinocytes upon treatment with supernatants and HA-U6N-EVs. (B) Migrated cells stained with crystal violet dye after 48 h (B1), and the migration promotion quantification of EVs among (B2) fibroblasts, (B3) endothelial cells, (B4) keratinocytes. The results were compared between corresponding EVs group to others (red * represented lower and black * represented higher). (C1) Brightfield images of HUVECs incubated on matrix adhesive and (C2) quantification of microvessels number among endothelial cells. The results were compared between EVs group to the control group. Results are mean \pm SD ($n = 3$). Statistical analyses were performed by unpaired parametric test with Welch's correction. Statistical differences: * $p < 0.05$; ** $p < 0.01$; *** $p < 0.001$; **** $p < 0.0001$. (For interpretation of the references to colour in this figure legend, the reader is referred to the web version of this article.)

longer and smoother kinetics of EVs release, enabling a higher amount of EVs to be applied throughout the entire treatment period compared to a single EVs administration. Additionally, soluble factors such as FGF could be detected in the cell supernatant of UCMSCs, which could be one of the cell viability promotion factors. Nevertheless, the FGF concentration didn't decrease significantly after HA-U6N enrichment, while the concentration in the elution product from HA-U6N-EVs composite hydrogel was similar as that from size exclusion column (Fig. S6). These findings revealed the specifically EVs adsorption and desorption ability of HA-U6N, together with the elimination of cytokines influences in the subsequent experiments. In summary, this study showcased the promising potential of HA-U6N-EVs composite hydrogel as an effective and efficient delivery system for MSC-EVs in wound healing applications. The combination of HA-U6N with MSC-EVs offers a novel and innovative approach to enhance the therapeutic effects of EVs and improve the treatment of chronic wounds, bringing us one step closer to developing advanced and effective wound healing therapies.

3.4. Wound healing efficacy of MSC-EVs released from HA-U6N-EVs composite hydrogel

Afterwards, we proceeded to investigate whether HA-U6N-EVs could promote the healing of diabetic full-thickness wounds or not. To do this, we grouped and modeled SD rats according to the experimental design shown in Fig. 4A. The rats exhibited significant weight loss after STZ injection, along with excessive drinking and urination, further

confirming the successful induction of diabetes. Blood glucose measurements also confirmed the establishment of diabetes in the rats. After anesthesia, full-thickness wounds were created on both sides of the rats' back using surgical scissors, and wound treatments were administered based on the seven assigned groups. The progress of wound healing was monitored by measuring the wound area on day 5 and day 10 post-treatment. Remarkably, rats treated with MSC-EVs exhibited a significant acceleration of wound closure on day 5, while the wound healing progress in the negative control group was unsatisfactory. The wound healing results on day 10 showed similar findings to those observed on day 5 (Fig. 4B). Furthermore, statistical analysis of wound healing rates further confirmed the superior healing efficiency of MSC-EVs, especially when continuously released after enrichment by HA-U6N, compared to the other treatment groups (Fig. 4C). These results strongly suggest that HA-U6N-EVs significantly enhance the healing of diabetic type I full-thickness wounds. The continuous release of MSC-EVs facilitated by HA-U6N offers an accelerating therapeutic approach for the treatment of chronic wounds, particularly in diabetic patients where wound healing can be particularly challenging.

Subsequent histology analyses were performed to evaluate the wound healing process at the tissue level (Fig. 5A). On day 5 post-wounding, the wounds treated with PBS displayed a significant amount of cytoplasm on the surface of the skin tissue, while inflammatory cells were infiltrating beneath the wound. The tissue surface still showed signs of inflammation at day 10, with slow progress in fibrosis and angiogenesis within the tissue. Wounds treated with HA or HA-U6N

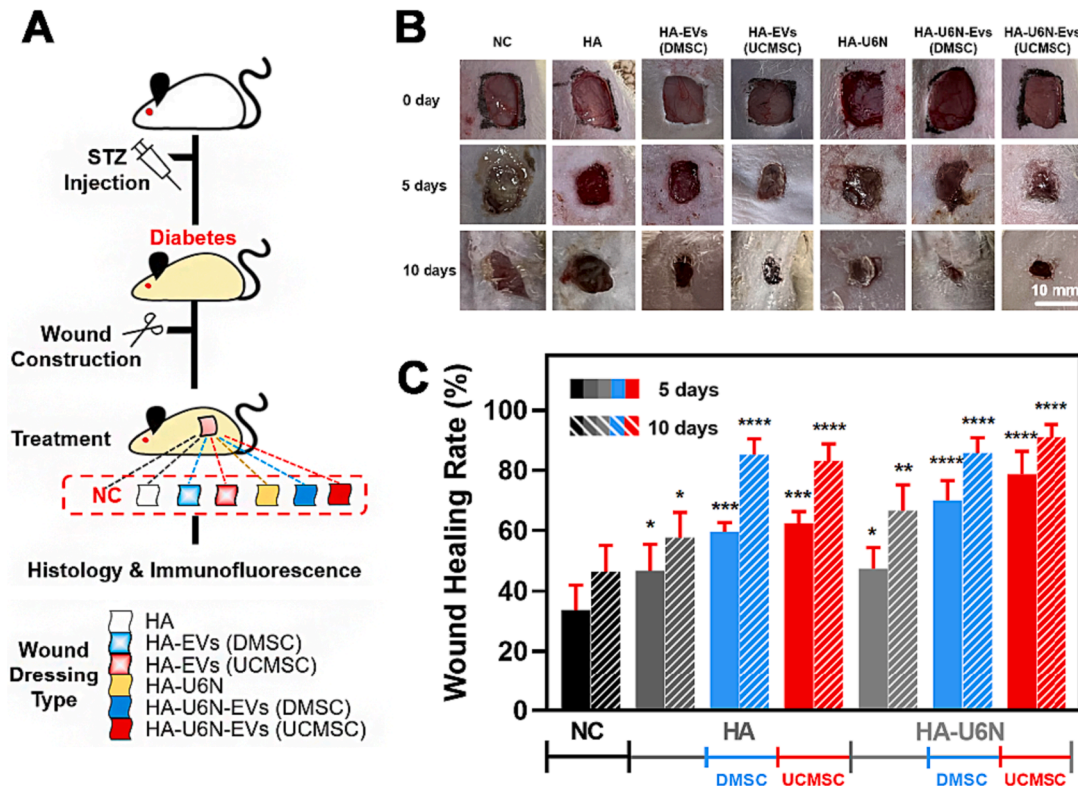


Fig. 4. Healing efficacy of HA-U6N-EVs composite hydrogel in type I diabetic chronic wounds. (A) Schematic representation of wound modeling in diabetic rats and further treatment strategies design *in vivo*. (B) Representative images of wounds in diabetic rats at 0 day, 5 days, and 10 days after treatment. (C) Percentage of wound healing rate after treatment with different strategies. Results are mean \pm SD ($n = 6$). Statistical analyses were performed by unpaired parametric test with Welch's correction, the results of day 5 and day 10 were compared correspondingly. Statistical differences: * $p < 0.05$; ** $p < 0.01$; *** $p < 0.001$; **** $p < 0.0001$.

exhibited keratosis on the surface at day 5, but internal inflammation was still evident. By day 10, the wound healing progress in these groups appeared better than the negative control (NC) group, showing some degree of epithelialization and extracellular matrix reorganization, but inflammation persisted internally. In contrast, the wound healing progress was much more promising in groups treated with HA-DMSC-EVs or HA-UCMSC-EVs. MSC-EVs effectively promoted the wound healing progress on the wound surface, with obvious wound contraction and remodeling by day 10. Interestingly, wounds treated with HA-U6N-EVs (both DMSC-EVs and UCMSC-EVs) displayed the highest levels of epithelialization, fibroblast proliferation, and extracellular matrix reorganization at day 5 compared to other groups. Moreover, their wound remodeling was also superior to all other groups at day 10. Overall, these histological findings suggest that HA-U6N-EVs, including both DMSC-EVs and UCMSC-EVs, significantly enhance wound healing progress at both early and later stages, making them promising candidates for effective wound healing therapies. Wound healing scores which were calculated according to Table S2 also reflected the superior therapeutic performance of HA-U6N-EVs composite hydrogels (Fig. 5B).

Correspondingly, the expression levels of Keratin-14 and Keratin-5 in the HA-U6N-EVs groups were higher than in other groups at day 10, indicating improved epithelialization due to the continuous release of EVs on the wound. Additionally, the expression level of α -SMA reflects the degree of fibroblast recruitment, and the expression level of CD31 is associated with angiogenesis during the wound healing process. As shown in Fig. 5C and D, wounds treated with HA-U6N-UCMSC-EVs showed the highest expression level of CD31 compared to other groups, while exhibiting a relatively lower expression level of α -SMA compared to the HA-U6N-DMSC-EVs group after 10 days. Meanwhile, the expression levels of Keratin-14 and Keratin-5 in the HA-U6N-EVs groups were higher than in other groups at day 10, indicating improved epithelialization due to the continuous release of EVs on the

wound. Additionally, the expression level of α -SMA reflects the degree of fibroblast recruitment, and the expression level of CD31 is associated with angiogenesis during the wound healing process. After 10 days, wounds treated with HA-U6N-UCMSC-EVs showed the highest expression level of CD31 compared to other groups, while exhibiting a relatively lower expression level of α -SMA compared to the HA-U6N-DMSC-EVs group. Thus, our *in vivo* results revealed the importance of continuous release of MSC-EVs in wound healing, characterized by accelerated skin re-epithelialization, fibroblast recruitment, and neo-vascularization. Furthermore, the delivery of MSC-EVs from hydrogels during wound healing enhanced tissue regeneration. This was confirmed at two different levels: through delivery from HA hydrogel and by the utilization of HA-U6N hydrogel, which allowed for continuous release of EVs, providing a promising approach for effective wound healing therapies.

Additionally, the number and polarization of macrophages in the wounds could reflect the level of inflammation in the tissue after treatment. The fluorescence of iNOS could represent the M1 macrophages with pro-inflammatory effects, while the fluorescence of CD206 could represent the M2 macrophages with anti-inflammatory effects. As shown in Fig. S7, the fluorescence intensity of iNOS in HA group was slightly higher than that in negative control group, whereas the numbers of M1 macrophages in MSC-EVs treated groups decreased significantly. Besides, the numbers of M2 macrophages increased significantly of all experimental groups comparing with negative control group. The M1/M2 ratio further indicated the inflammatory state, which all the experimental groups showed significant improvement in inflammation levels comparing with negative control group. Furthermore, both numbers of M1 and M2 macrophages were relatively high in wounds only treated with HA or HA-U6N, while the M1/M2 ratio was decreased significantly after MSC-EVs treatment. Moreover, wounds treated with HA-UCMSC-EVs, HA-U6N-DMSC-EVs, and HA-U6N-UCMSC-EVs after 5 days showed less hydroxyl radical inhibiting levels than other groups, while

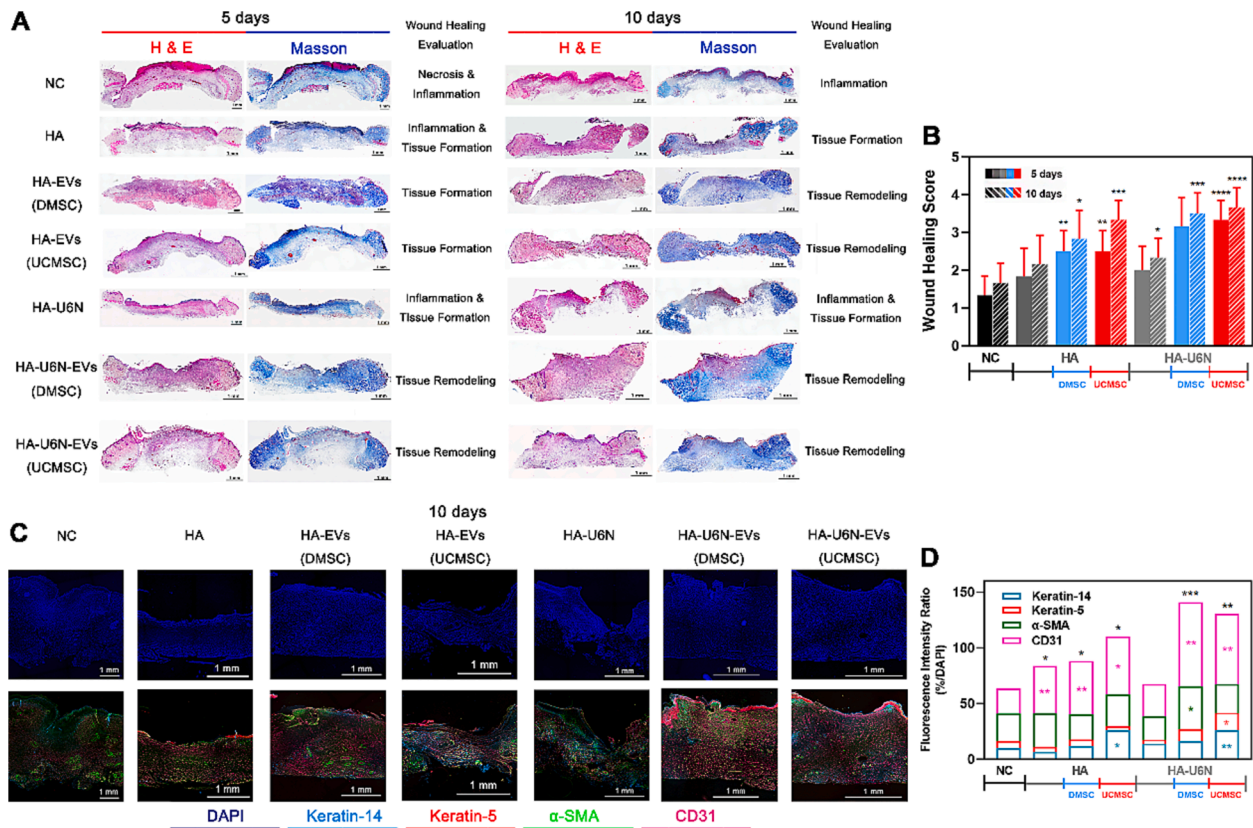


Fig. 5. Histology investigation of wounds after treatments. (A) Wounds stained by H&E and Masson in each group were scanned to comparing the healing efficacy of HA-U6N-EVs composite hydrogel. (B) Wound healing score calculation based on histology investigation of wounds after treatments. Results were mean \pm SD, $n = 6$. (C) Representative fluorescence images of Keratin-14, Keratin-5, α -SMA, and CD31 in wounds with different treatments after 10 days. (D) Relative fluorescence intensity calculation of Keratin-14, Keratin-5, α -SMA, and CD31 in wounds with different treatments after 10 days. Results were mean \pm SD, $n = 3$. Statistical analyses were performed by unpaired parametric test with Welch's correction, the results were compared between each group to negative control group. Statistical differences: * $p < 0.05$; ** $p < 0.01$; *** $p < 0.001$; **** $p < 0.0001$.

the SOD enzyme activities in HA-U6N-EVs groups were lower than others, correspondingly (Fig. S8). These findings demonstrated the lower inflammation level and oxidative stress level after MSC-EVs treatment, which also highlighted the EVs enrichment and sustained releasing character of HA-U6N comparing with HA. Notably, HA or HA-U6N themselves could hardly inhibit the inflammation and oxidative stress on diabetic wounds, so that the functions and utilizations of the active ingredients were the key of the hydrogel in accelerating chronic wound healing. Finally, the organs including heart, liver, spleen, lung, and kidney after HA-U6N-EVs treatment showed no obvious pathological changes, while the zirconium residual of each tissue sample was relatively low even after the incubation of HA-U6N upon the wound (Figs. S9 and S10). Zirconium is a non-toxic element and can be excreted from urine. Therefore, the very low dose of zirconium diffused into wounds from HA-U6N was relatively safe.

3.5. Distribution of miRNAs contained in MSC-EVs during wound healing

The functions of MSCs in accelerating wound healing are partially mediated by EVs. The miRNAs contained in EVs can be delivered into skin recipient cells, promoting downstream cascade signaling changes, which are beneficial for wound healing. In this study, several miRNAs were compared between the two types of MSC-EVs, both of which have been considered to have positive effects on wound healing. Fig. 6A showed that the abundance of miR-21-5p, miR-125b-5p, and miR-150-5p in UCMSC-EVs was relatively higher compared to DMSC-EVs. On the other hand, the abundance of miR-23a-3p and miR-146a-5p in DMSC-EVs was higher than in UCMSC-EVs. These miRNAs have

different roles in wound healing. For instance, miR-21 and miR-150 can inhibit PTEN expression, leading to increased corneal epithelial wound repair. MiR-125 can inhibit p53 protein expression, reducing hypoxia-induced cell apoptosis. In contrast, miR-23 and miR-146 are mainly involved in suppressing myofibroblast differentiation through TGF- β inhibition. Additionally, several miRNAs common in MSC-EVs showed relatively low abundance in both UCMSC-EVs and DMSC-EVs.

Next, the miRNAs with relatively high abundance in UCMSC-EVs and DMSC-EVs were amplified using qPCR in the skin tissues to investigate the onset time and concentration of MSC-EVs in the wounds. Three miRNAs, including miR-21-5p, miR-125b-5p, and miR-150-5p, showed significant differences between the groups. The distribution of miR-21 derived from HA-U6N-UCMSC-EVs was significantly higher than that from HA-UCMSC-EVs at both day 5 and day 10 in the skin tissues. The performance of DMSC-EVs was relatively inferior compared to UCMSC-EVs. Additionally, the distribution of miR-21 at day 10 decreased rapidly in both the HA-DMSC-EVs group and HA-UCMSC-EVs group compared to the distribution at day 5, while there was no significant difference among HA-U6N groups over time. Similarly, the distribution of miR-125b in the HA-U6N-EVs composite hydrogel-treated groups was significantly higher than that in the HA-EVs-treated groups, with UCMSC-EVs treated groups showing better performance than DMSC-EVs groups. Slight differently, the distribution of miR-150 after EVs-treated was significantly higher than that in no EVs treated groups, but the abundance differences between DMSC-EVs and UCMSC-EVs were not significant (Fig. 6B–D). In contrast, miR-23a and miR-146a, which were highly abundant in DMSC-EVs, showed no significant difference after MSC-EVs treatment compared to the control groups (Fig. S11). Of note,

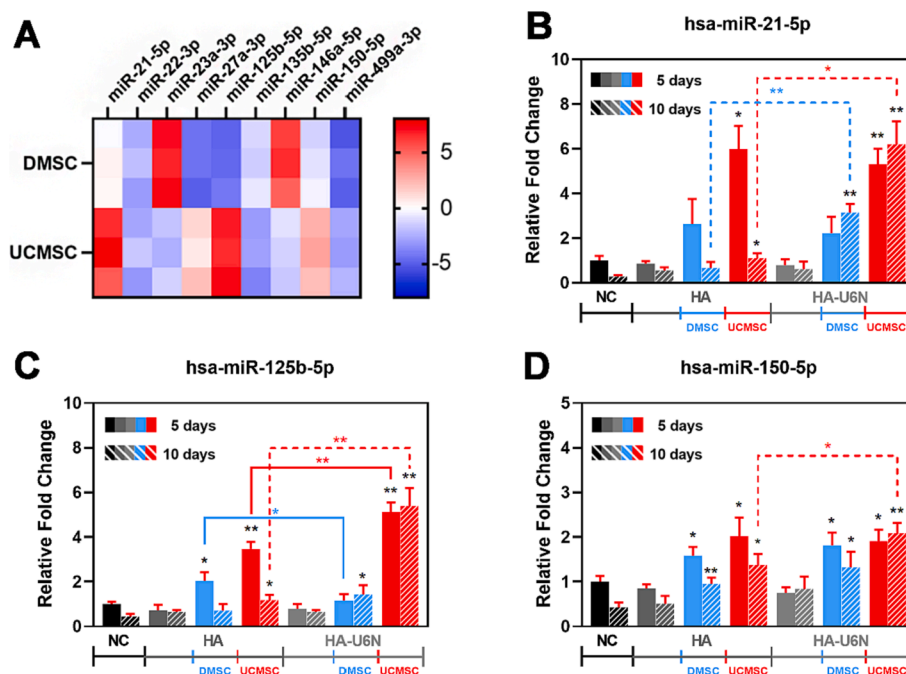


Fig. 6. Abundance of miRNAs delivered from EVs in wounds. (A) Abundance comparison of miRNAs involved in wound healing delivered from DMSC-EVs and UCMSC-EVs. Red represented the lower Ct value, whereas blue represented higher Ct value of corresponding miRNA than the average Ct value. (B–D) Abundance of (B) hsa-miR-21-5p, (C) hsa-miR-125b-5p, (D) hsa-miR-150-5p in wounds treated with different strategies. Results are mean \pm SD ($n = 3$). Statistical analyses were performed by unpaired parametric test with Welch's correction, the results of day 5 and day 10 in each group were compared respectively, whereas the results of HA-EVs groups and HA-U6N-EVs groups were compared additionally. Statistical differences: * $p < 0.05$; ** $p < 0.01$. (For interpretation of the references to colour in this figure legend, the reader is referred to the web version of this article.)

miR-21, miR-125b, and miR-150 are more relevant to proliferation [32–34], whereas miR-23a and miR-146a are involved in differentiation [35,36]. Proliferation is more critical than differentiation in view of the different needs of various stages during wound healing, especially in the recovery of chronic wounds. Therefore, miRNAs involved in proliferation showed better preservation in the skin tissues. Moreover, the distribution of miR-21, miR-125b, and miR-150 in wound tissues after treatments was corresponded to the abundance of miRNAs in DMSC-EVs and UCMSC-EVs mentioned above. Furthermore, UCMSC-EVs demonstrated superior performance compared to DMSC-EVs for chronic wound healing due to their more efficient inclusion of relevant miRNAs.

4. Conclusion

In summary, this study developed a novel MOFs hydrogel by cross-linking HA and U6N. The HA-U6N hydrogel effectively enriched EVs from cell supernatant and continuously released them through PBS elution. The HA-U6N-EVs composite hydrogel demonstrated accelerated wound healing due to the higher embedding of MSC-EVs and longer release term compared to other treatments. Moreover, the investigation of miRNAs contained in DMSC-EVs and UCMSC-EVs shed light on the characteristics of MSC-EVs in the context of wound healing. These findings highlight the potential of the HA-U6N-EVs composite hydrogel as a promising strategy for chronic wound healing. Meanwhile, the preparation of hydrogels into self-assembly or self-degradation modes, such as utilizing the higher blood glucose concentration at the wound site of diabetic ulcer, may be more in line with the needs of patients for hydrogel dressings, and will also be an interesting research direction.

Fundings

This study was supported by National Natural Science Foundation of China (NSFC) [81571213 and 82070459 (Bin Wang)], Key Project of Jiangsu Province (Grant No. BE2020765) (Bin Wang), and Project of

Modern Hospital Management and Development Institute, Nanjing University/Aid project of Nanjing Drum Tower Hospital Health, Education & Research Foundation (NDYG2020030) (Bin Wang). Jiangsu Biobank of Clinical Resources (BM2015004). Additionally, Key Project supported by Medical Science and technology development Foundation, and Nanjing Department of Health (YKK20071), Project of Modern Hospital Management and Development Institute, Nanjing University (NDYG2021009) (Hui Yang) also supported this study.

CRediT authorship contribution statement

Wang Pan: Writing – review & editing, Writing – original draft, Visualization, Validation, Software, Project administration, Methodology, Investigation, Formal analysis, Data curation, Conceptualization. **Wenqing Wang:** Writing – original draft, Visualization, Validation, Methodology, Investigation, Formal analysis, Data curation. **Peng Wang:** Supervision, Software, Resources, Investigation, Formal analysis. **Dong Chen:** Validation, Methodology, Investigation. **Shuo Liu:** Methodology, Investigation, Data curation. **Likun Zhang:** Resources, Investigation. **Ziyu Wang:** Resources, Investigation. **Hui Yang:** Resources, Funding acquisition. **Yuanyuan Xie:** Resources, Methodology. **Feifei Huang:** Resources, Methodology. **Guohua Zhou:** Writing – review & editing, Writing – original draft, Supervision, Resources, Methodology, Formal analysis, Conceptualization. **Bin Wang:** Writing – review & editing, Writing – original draft, Supervision, Resources, Project administration, Funding acquisition, Formal analysis, Conceptualization.

Declaration of competing interest

The authors declare that they have no known competing financial interests or personal relationships that could have appeared to influence the work reported in this paper.

Data availability

Data will be made available on request.

Appendix A. Supplementary data

Supplementary data to this article can be found online at <https://doi.org/10.1016/j.matdes.2024.112688>.

References

- [1] A.J. Singer, R.A. Clark, Cutaneous wound healing, *N. Engl. J. Med.* 341 (10) (1999) 738–746.
- [2] S. Shakya, Y. Wang, J.A. Mack, E.V. Maytin, Hyperglycemia-induced changes in hyaluronan contribute to impaired skin wound healing in diabetes: review and perspective, *Int. J. Cell Biol.* 2015 (2015) 701738.
- [3] L.J. Born, K.H. Chang, P. Shoureshi, F. Lay, S. Bengali, A.T.W. Hsu, S.N. Abadchi, J. W. Harmon, S.M. Jay, HOTAIR-loaded mesenchymal stem/stromal cell extracellular vesicles enhance angiogenesis and wound healing, *Adv. Healthc. Mater.* 11 (5) (2022) e2002070.
- [4] G. Marfia, S.E. Navone, C. Di Vito, N. Ughi, S. Tabano, M. Miozzo, C. Tremolada, G. Bolla, C. Crotti, F. Ingegnoli, P. Rampini, L. Riboni, R. Gualtierotti, R. Campanella, Mesenchymal stem cells: potential for therapy and treatment of chronic non-healing skin wounds, *Organogenesis* 11 (4) (2015) 183–206.
- [5] H.J. Kim, J.S. Park, Usage of human mesenchymal stem cells in cell-based therapy: advantages and disadvantages, *Dev. Reprod.* 21 (1) (2017) 1–10.
- [6] L. Mazini, L. Rochette, B. Admou, S. Amal, G. Malka, Hopes and limits of adipose-derived stem cells (ADSCs) and mesenchymal stem cells (MSCs) in wound healing, *Int. J. Mol. Sci.* 21 (4) (2020).
- [7] C. Wang, M. Wang, T. Xu, X. Zhang, C. Lin, W. Gao, H. Xu, B. Lei, C. Mao, Engineering bioactive self-healing antibacterial exosomes hydrogel for promoting chronic diabetic wound healing and complete skin regeneration, *Theranostics* 9 (1) (2019) 65–76.
- [8] R. Kalluri, V.S. LeBleu, The biology, function, and biomedical applications of exosomes, *Science* 367 (6478) (2020).
- [9] D.H. Ha, H.K. Kim, J. Lee, H.H. Kwon, G.H. Park, S.H. Yang, J.Y. Jung, H. Choi, J. H. Lee, S. Sung, Y.W. Yi, B.S. Cho, Mesenchymal stem/stromal cell-derived exosomes for immunomodulatory therapeutics and skin regeneration, *Cells* 9 (5) (2020).
- [10] S.E.L. Andaloussi, I. Mager, X.O. Breakefield, M.J. Wood, Extracellular vesicles: biology and emerging therapeutic opportunities, *Nat. Rev. Drug Discov.* 12 (5) (2013) 347–357.
- [11] C. Zhou, B. Zhang, Y. Yang, Q. Jiang, T. Li, J. Gong, H. Tang, Q. Zhang, Stem cell-derived exosomes: emerging therapeutic opportunities for wound healing, *Stem Cell Res. Ther.* 14 (1) (2023) 107.
- [12] R. Tutuianu, A.M. Rosca, D.M. Iacomi, M. Simionescu, I. Titorencu, Human mesenchymal stromal cell-derived exosomes promote in vitro wound healing by modulating the biological properties of skin keratinocytes and fibroblasts and stimulating angiogenesis, *Int. J. Mol. Sci.* 22 (12) (2021).
- [13] V. Budnik, C. Ruiz-Canada, F. Wendler, Extracellular vesicles round off communication in the nervous system, *Nat. Rev. Neurosci.* 17 (3) (2016) 160–172.
- [14] C.P. Lai, O. Mardini, M. Ericsson, S. Prabhakar, C. Maguire, J.W. Chen, B. A. Tannous, X.O. Breakefield, Dynamic biodistribution of extracellular vesicles in vivo using a multimodal imaging reporter, *ACS Nano* 8 (1) (2014) 483–494.
- [15] Y. Zhang, Y. Xie, Z. Hao, P. Zhou, P. Wang, S. Fang, L. Li, S. Xu, Y. Xia, Umbilical mesenchymal stem cell-derived exosome-encapsulated hydrogels accelerate bone repair by enhancing angiogenesis, *ACS Appl. Mater. Interfaces* 13 (16) (2021) 18472–18487.
- [16] Z. Huang, S. Liu, J. Xu, L. Yin, F. Sun, N. Zhou, G. Ouyang, Fabrication of 8-aminocaprylic acid doped UIO-66 as sensitive solid-phase microextraction fiber for nitrosamines, *Talanta* 178 (2018) 629–635.
- [17] Z. Fang, B. Bueken, D.E. De Vos, R.A. Fischer, Defect-engineered metal-organic frameworks, *Angew. Chem. Int. Ed. Engl.* 54 (25) (2015) 7234–7254.
- [18] K.M. Choi, D. Kim, B. Rungtaweeworant, C.A. Trickett, J.T. Barmanbek, A. S. Alshammari, P. Yang, O.M. Yaghi, Plasmon-enhanced photocatalytic CO(2) conversion within metal-organic frameworks under visible light, *J. Am. Chem. Soc.* 139 (1) (2017) 356–362.
- [19] N. Manousi, D.A. Giannakoudakis, E. Rosenberg, G.A. Zachariadis, Extraction of metal ions with metal-organic frameworks, *Molecules* 24 (24) (2019).
- [20] W. Pan, X. Wang, X. Ma, Y. Chu, S. Pang, Y. Chen, X. Guan, B. Zou, Y. Wu, G. Zhou, Postsynthetic modification of the magnetic zirconium-organic framework for efficient and rapid solid-phase extraction of DNA, *ACS Appl. Mater. Interfaces* 13 (42) (2021) 50309–50318.
- [21] Z. Wang, Y. Fu, Z. Kang, X. Liu, N. Chen, Q. Wang, Y. Tu, L. Wang, S. Song, D. Ling, H. Song, X. Kong, C. Fan, Organelle-specific triggered release of immunostimulatory oligonucleotides from intrinsically coordinated DNA-metal-organic frameworks with soluble exoskeleton, *J. Am. Chem. Soc.* 139 (44) (2017) 15784–15791.
- [22] X. Wang, Y. Wu, J. Shan, W. Pan, S. Pang, Y. Chu, X. Ma, B. Zou, Y. Li, H. Wu, G. Zhou, Lipid membrane anchoring and highly specific fluorescence detection of cancer-derived exosomes based on postfunctionalized zirconium-metal-organic frameworks, *Biochem. Biophys. Res. Commun.* 609 (2022) 69–74.
- [23] Y. Xi, J. Ge, Y. Guo, B. Lei, P.X. Ma, Biomimetic elastomeric polypeptide-based nanofibrous matrix for overcoming multidrug-resistant bacteria and enhancing full-thickness wound healing/skin regeneration, *ACS Nano* 12 (11) (2018) 10772–10784.
- [24] G. Sharifzadeh, H. Hosseinkhani, Biomolecule-responsive hydrogels in medicine, *Adv. Healthc. Mater.* 6 (24) (2017).
- [25] S. Yang, L. Peng, O.A. Syzgantseva, O. Trukhina, I. Kochetygov, A. Justin, D.T. Sun, H. Abedini, M.A. Syzgantseva, E. Oveisi, G. Lu, W.L. Queen, Preparation of highly porous metal-organic framework beads for metal extraction from liquid streams, *J. Am. Chem. Soc.* 142 (31) (2020) 13415–13425.
- [26] Z. Bai, Q. Liu, H. Zhang, J. Yu, R. Chen, J. Liu, D. Song, R. Li, J. Wang, Anti-biofouling and water-stable balanced charged metal organic framework-based polyelectrolyte hydrogels for extracting uranium from seawater, *ACS Appl. Mater. Interfaces* 12 (15) (2020) 18012–18022.
- [27] S. Yan, Q. Zhang, J. Wang, Y. Liu, S. Lu, M. Li, D.L. Kaplan, Silk fibroin/chondroitin sulfate/hyaluronic acid ternary scaffolds for dermal tissue reconstruction, *Acta Biomater.* 9 (6) (2013) 6771–6782.
- [28] J. Zhu, F. Li, X. Wang, J. Yu, D. Wu, Hyaluronic acid and polyethylene glycol hybrid hydrogel encapsulating nanogel with hemostasis and sustainable antibacterial property for wound healing, *ACS Appl. Mater. Interfaces* 10 (16) (2018) 13304–13316.
- [29] H. Bai, N. Kyu-Cheol, Z. Wang, Y. Cui, H. Liu, H. Liu, Y. Feng, Y. Zhao, Q. Lin, Z. Li, Regulation of inflammatory microenvironment using a self-healing hydrogel loaded with BM-MSCs for advanced wound healing in rat diabetic foot ulcers, *J. Tissue Eng.* 11 (2020), 2041731420947242.
- [30] D. Cukjati, S. Rebersek, D. Miklavcic, A reliable method of determining wound healing rate, *Med. Biol. Eng. Comput.* 39 (2) (2001) 263–271.
- [31] T. Li, M. Xia, Y. Gao, Y. Chen, Y. Xu, Human umbilical cord mesenchymal stem cells: an overview of their potential in cell-based therapy, *Expert Opin. Biol. Ther.* 15 (9) (2015) 1293–1306.
- [32] X. Liu, X. Li, G. Wu, P. Qi, Y. Zhang, Z. Liu, X. Li, Y. Yu, X. Ye, Y. Li, D. Yang, Y. Teng, C. Shi, X. Jin, S. Qi, Y. Liu, S. Wang, Y. Liu, F. Cao, Q. Kong, Z. Wang, H. Zhang, Umbilical cord mesenchymal stem cell-derived small extracellular vesicles deliver miR-21 to promote corneal epithelial wound healing through PTEN/PI3K/Akt pathway, *Stem Cells Int.* 2022 (2022) 1252557.
- [33] X.F. Zhang, T. Wang, Z.X. Wang, K.P. Huang, Y.W. Zhang, G.L. Wang, H.J. Zhang, Z.H. Chen, C.Y. Wang, J.X. Zhang, H. Wang, Hypoxic ucMSC-secreted exosomal miR-125b promotes endothelial cell survival and migration during wound healing by targeting TP53INP1, *Mol. Ther. Nucl. Acids* 26 (2021) 347–359.
- [34] H. Henriques-Antunes, R.M.S. Cardoso, A. Zonari, J. Correia, E.C. Leal, A. Jimenez-Balsa, M.M. Lino, A. Barradas, I. Kostic, C. Gomes, J.M. Karp, E. Carvalho, L. Ferreira, The kinetics of small extracellular vesicle delivery impacts skin tissue regeneration, *ACS Nano* 13 (8) (2019) 8694–8707.
- [35] Y. Zhang, J. Yan, Y. Liu, Z. Chen, X. Li, L. Tang, J. Li, M. Duan, G. Zhang, Human amniotic fluid stem cell-derived exosomes as a novel cell-free therapy for cutaneous regeneration, *Front. Cell Dev. Biol.* 9 (2021) 685873.
- [36] S.A. Eming, P. Martin, M. Tomic-Canic, Wound repair and regeneration: mechanisms, signaling, and translation, *Sci. Transl. Med.* 6 (265) (2014) 265sr6.